Towards the Modeling of Laminar to Turbulence Transition for Incompressible Flows

Ginevra Rubino* **and Michel Visonneau***
*ECN/CNRS, Nantes, France †
ginevra.rubino@ec-nantes.fr

1 Introduction

Nowadays, in the context of transition modeling, the CFD community is moving towards the so-called Local-Correlation based Transition Modeling (LCTM) concept. The main idea is to provide a set of generic transport equations built using local informations, based on experimental correlations and coupled with the already existing turbulence models. Within LCTM, the γ model, Menter et al. (2015), is the transition model that we are going to analyze.
The γ model is included in the class of transition models based on the intermittency concept and the use of only local informations to trigger the transition. Within LCTM, it is the only model Galilean invariant. The transport equation for the intermittency γ is:

$$\frac{\partial(\rho\gamma)}{\partial t}+\frac{\partial(\rho u_j\gamma)}{\partial x_j}=\underbrace{F_{\text{onset}}[F_{\text{length}}(\rho S(1-\gamma)\gamma)]}_{P_\gamma}-\underbrace{c_{a2}\rho\Omega\gamma F_{\text{turb}}(c_{e2}\gamma-1)}_{E_\gamma}+\frac{\partial}{\partial x_j}\Big[\Big(\mu+\frac{\mu_t}{\sigma_\gamma}\Big)\frac{\partial\gamma}{\partial x_j}\Big]. \tag{1}$$

E_γ and P_γ are the relaminarization/destruction term and production term, respectively. In the latter, the constant $F_{\text{length}}=100$ determines the magnitude of the production term, while F_{onset} is defined through an empirical correlation and it is meant to activate the production of intermittency inside the boundary layer, when the transition process starts. The definition of the correlation F_{onset} slightly changes according to the transition mechanism. It is based on the relation between the vorticity Reynolds number Re_v and the momentum thickness Re_{θ_c},

$$\frac{Re_V}{2.2Re_{\theta_c}}. \tag{2}$$

Experimentally, indeed, it was observed that transition occurs when $Re_V=\frac{\rho y^2 S}{\mu}$ reaches a critical value inside the boundary layer.
The critical Reynolds number is computed through the correlation $Re_{\theta_c}=f(Tu_L,\lambda_{\theta L})$, which depends on local quantities computed inside the boundary layer:

- the level of turbulence intensity inside the boundary layer is expressed as

$$Tu_L=\min\left(100\frac{\sqrt{2k/3}}{\omega y},100\right); \tag{3}$$

- the pressure gradient parameter λ_θ can be expressed exploiting the incompressibility constraint in 2D as

$$\lambda_\theta=\frac{\rho\theta^2}{\mu}\frac{dU}{dS}=-\frac{\rho\theta^2}{\mu}\frac{dV}{dy}, \tag{4}$$

  where $\frac{dU}{dS}$ is the flow acceleration in the stream-wise direction, at the edge of the boundary layer and $\frac{dV}{dy}$ is the derivative of the wall normal velocity component V in respect of the direction normal to the wall.

For a general geometry, $\frac{dV}{dy}$ can be computed as:

$$\frac{dV}{dy}\equiv\nabla(\mathbf{n}\cdot\mathbf{U})\cdot\mathbf{n}. \tag{5}$$

where $\mathbf{U}$ and $\mathbf{n}$ are the velocity and normal to the wall vectors, respectively.

Coupling with SST turbulence model. In the original $k-\omega$ SST turbulence model, the transport equation for the turbulence kinetic energy k is modified as it follows:

$$\frac{\partial(\rho k)}{\partial t}+\frac{\partial(\rho u_j k)}{\partial x_j}=P'_k+P_k^{\lim}-D'_k+\frac{\partial}{\partial x_j}\Big[\big(\mu+\sigma_k\mu_t\big)\frac{\partial k}{\partial x_j}\Big], \tag{6}$$

where the primary production term P'_k and the destruction term D'_k are redefined as

$$P'_k=\gamma P_k \text{ and } D'_k=\max(\gamma,0.1)\cdot D_k. \tag{7}$$

The term P_k in Eq.(7) is equal to $\mu_t S\,\Omega$, according to Kato-Launder modification. The additional term of production $P_k^{\lim}$ is added in order to make the transition prediction more reliable when it develops under low turbulence intensities.
Finally, the blending function F_1 is redefined in order to guarantee the use of $k-\omega$ formulation in the near wall region. In the presented work, γ model has been coupled with the 1994 version $k-\omega$ SST from Menter.
We are going to discuss a 2D and a 3D computation. The simulations presented in the following where computed using ISIS-CFD solver for incompressible flows.

2 2D-Flat Plate

With the purpose of evaluating the modeling error, we will present the results around a flat plate for $Re=10^7$ has been run. The inlet turbulence intensity is set to $Tu=0.536609\%$ and three different eddy viscosity ratios $\nu_t/\nu=\{270,280,290\}$ were tested in order to evaluate the input/parameter uncertainties. The simulations were run on a set of five geometrical similar structured O-grids provided by IST.
Multivariate Metrics. Following ASME V&V 20-2009, given a set of n validation points, we define the $n\times n$ covariance matrix $U_{\text{val}}=U_{\text{num}}+U_{\text{d}}+U_{\text{input}}$, whose entrances are the sum of the numerical, experimental and input uncertainties. Computed the comparison error $E=S-D$ (S numerical, D experimental) at each given point, we define the multivariate metric as

$$E_{\text{mv}}=\sqrt{E^T U_{\text{val}}^{-1}E}. \tag{8}$$

Assuming that each estimate of the comparison E and u_{val} is distributed as a Gaussian, we can define a reference value for the multivariate metric $E_{ref}=\sqrt{n+\sqrt{2n}}$.
Through the multivariate metrics we can state that if E_{mv}/E_{ref} is larger than one, it is an indication that the model is not able to reproduce the experimental data within the range of the validation uncertainty at each set point.
Results. In Figures (1) and (2) are presented the C_f and the velocity profile V_x/V at $X/L=0.02035$ (transition region) with the estimated error bars next to the correspondent comparison errors $E(C_f)$ and $E(V_x/V)$. The multivariate metrics are reported in Tables (1) and (2).
In Fig.(1), we plot the skin friction profile all along the flat plate. The main discrepancies between the model and the experimental data are in the transition region: the model predicts higher values of skin friction in the transition region in respect of the experiments. It is interesting that there is no overlapping between the numerical and experimental error bars in this region and this reflects the high multivariate metrics computed in this zone (Table(1)). The source of this high uncertainty is related to the lack of accuracy of the model, but also to the lack of accuracy of the experimental data. In addition, the experimental uncertainty is very low and that could be an additional reason of the error bars non-overlapping. The quantitative discrepancies between the experimental data and the computations in the laminar region are related to the fact that the values of turbulence kinetic energy at the leading edge between computations and experiments do not match, despite the freestream turbulence intensity at the inlet of the computational domain has been tuned in order to have the experimental value of k at the leading edge. Minor differences are observed in the turbulence region.
In general, the numerical uncertainty is the biggest contributor to the matrix U_{val}. Indeed, despite we

obtain reasonable value of the order of accuracy p, which is above 1.6, the numerical uncertainty percentage is high because the meshes are not in the asymptotic range. For this reason, we are planning to run new simulations on a set of finer meshes.
In Fig.(2), the velocity profile V_x/V at $X/L = 0.02035$ in the transition region is plotted. We notice that numerically the production term of turbulence kinetic energy is too strong, slightly accelerating the transition process in the boundary layer. As discussed for the skin friction distribution, the modeling error results to be higher in the transition region in respect of the laminar and turbulence one, as we can observe from the multivariate metrics computed at three different slices in the three different regions reported in Table(2).

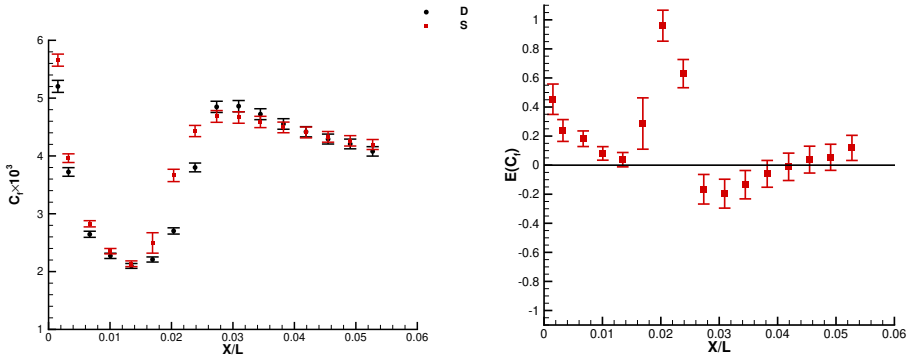

(a) Numerical (S) and Experimental (D) $C_f \times 10^3$ profiles on the flat plate surface.

(b) Comparison error $E(C_f)$.

Fig. 1: Error bars for the Skin Friction C_f.

	Laminar Region	Transition Region	Turbulent Region	Total
E/E_{ref}	2.34	4.03	0.71	2.89

Table 1: Multivariate metric for the skin friction in different regions and all over the flat plate.

	$X/L = 0.01006$	$X/L = 0.02035$	$X/L = 0.05273$
E/E_{ref}	1.58	4.56	1.73

Table 2: Multivariate metric for the velocity profiles at different positions along the flat plate.

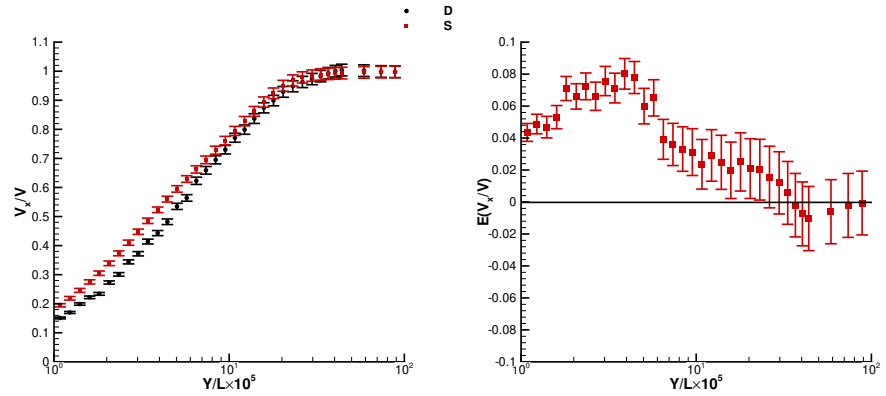

Fig. 2: V_x/V and $E(V_x/V)$ with error bars in the transition region at $X = 0.02035L$.

3 γ Model - Towards 3D

The crossflow effects in the γ model are included through the C1-correlation proposed by Arnal (1984). According to the correlation, the crossflow transition occurs when the following criterion is met:

$$\frac{Re_{\delta^*_{\delta 2t}}}{150 f(H_S)} \geqslant 1, \tag{9}$$

where $Re_{\delta^*_{\delta 2}}$ is the crossflow Reynolds number and $f(H_s)$ is a function of the shape factor.
The C1 criterion is locally formulated and implemented as:

$$T_{\text{C1local}} = \frac{C_{RSF}}{150}(G\Psi Re_V) > 1. \tag{10}$$

Each function in the parenthesis in (10) accounts for a specific effect:

- G accounts for the influence of the pressure gradient, i.e. the shape factor;
- the indicator Ψ is a non-dimensional measure of the local crossflow strength in respect of the streamwise strength and it is defined as:

$$\Psi = \left|\overrightarrow{n} \cdot \nabla\left(\frac{\overrightarrow{\omega}}{|\overrightarrow{\omega}|}\right)\right| y, \tag{11}$$

  with $\overrightarrow{n}$ wall normal and $\overrightarrow{\omega}$ vorticity. The vorticity $\overrightarrow{\omega}$ and its derivatives in the normal direction are used because they are the only physical quantities which describe the 3-dimensionality of the boundary layer;
- Re_V is the local vorticity Reynolds number.

The crossflow transition is then triggered through the onset function

$$F_{\text{onset,CF}} = \min[\max[100(T_{\text{C1local}} - 1), 0], 1]. \tag{12}$$

3.1 6:1 Prolate Spheroid

The model described above was tested on the 6:1 prolate spheroid configuration. We compared two different simulations with the experimental results performed in the low speed wind tunnel at DLR Gottingen, Kreplin et al. (1985). The simulations have run for $\alpha = 15°$, $Re = 6.5 \times 10^6$. Under these conditions Tolmienn-Schlichting transition is observed on the leeward side next to the symmetry plane, while the transition in the middle and windward side is dominated by crossflow instabilities.
We have set to different combinations of values of turbulence intensity and eddy viscosity ratios at the inlet: (1) $Tu = 0.15\%$ and $\frac{\nu_t}{\nu} = 21$, (2) $Tu = 0.5\%$ and $\frac{\nu_t}{\nu} = 250$. The first combination leads to $\omega = 1$ and it represents an unphysical way to reduce the turbulence kinetic energy decay ahead of the leading edge; the second combination mathematically results in a value of k at the leading edge as the one of the experiments. Simulations have been run on half model. The grid, provided by DLR, is unstructured with a total number of nodes $N = 53938$, of which 1253 on the spheroid surface, with $y^+ = 1$.
Results. In Fig.(3) are shown the experimental and the numerical skin friction distributions on the surface for the different inlet conditions. The differences between computations and experiments are huge: none of the computations is able to predict crossflow transition, because the crossflow criterion is never activated in the first cells next to the wall. In both cases, the model is predicting natural transition.
In Fig.(3b) and (4a), we observe the skin friction distribution for $Tu = 0.15\%$ and $\frac{\nu_t}{\nu} = 21$, on two different planes x-z and x-ϕ, where $0° \leqslant \phi \leqslant 180°$. On the leeward side, next to the symmetry plane, transition due to T-S waves occurs at about 10% of the spheroid length, upward in respect of the experiments. Indeed, experimentally, transition occurs along the isoline $C_f = 0.0025$, which are denoted by the black dots in Fig.(4). At about 10% of the spheroid length, we observe the upper side kink, which is less pronounced with respect to the experimental results. This discontinuity is present because of the change on

the transition mechanism, from T-S to crossflow instabilities. However, on the windward side the model does not predict any transition and the flow only transitions as it separates at the trailing edge, where the skin friction lines converge. Also the topology of the skin friction lines is questionable, indeed, because of the high angle of incidence, we were expecting the streamlines on the windward side to converge to the primary separation line upward with respect to what is predicted by the present computations.
In Fig.(3c) and (4b) another scenario is visible for $Tu = 0.5\%$ and $\frac{\nu_t}{\nu} = 250$. It is evident the extreme sensitivity of the model to the inlet parameters: an higher value of turbulence kinetic energy at the inlet results in a faster transition. This is the reason why the flow transitions at about 5% of the length the spheroid. The transition is due to a 2D mechanism, because neither in this case the crossflow criterion is ever activated as it has mentioned before. Nonetheless, this kind of behavior was not expected according to the experiments and it is allegedly due to a excessive numerical production of turbulence kinetic energy inside the boundary layer related to the computation of the velocity derivative normal to the wall.

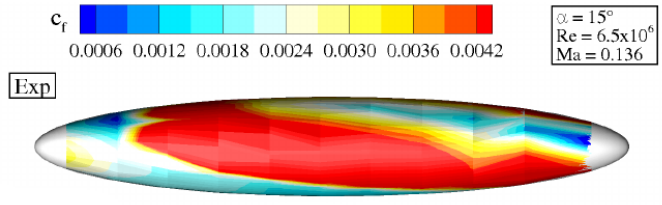

(a) Experimental Results from Grabe et al. (2016).

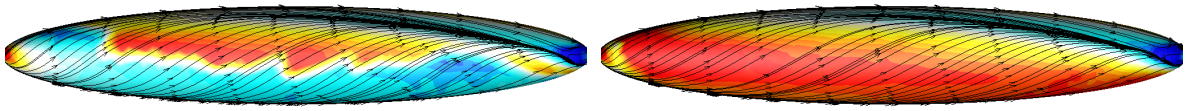

(b) Numerical results for $\frac{\nu_t}{\nu} = 21$ and $Tu = 0.0015$ at the inlet.(c) Numerical results for $\frac{\nu_t}{\nu} = 250$ and $Tu = 0.005$ at the inlet.

Fig. 3: Top views of experimental and numerical results of the crossflow transition around a spheroid for $\alpha = 15°$. Skin-friction lines are added to computations.

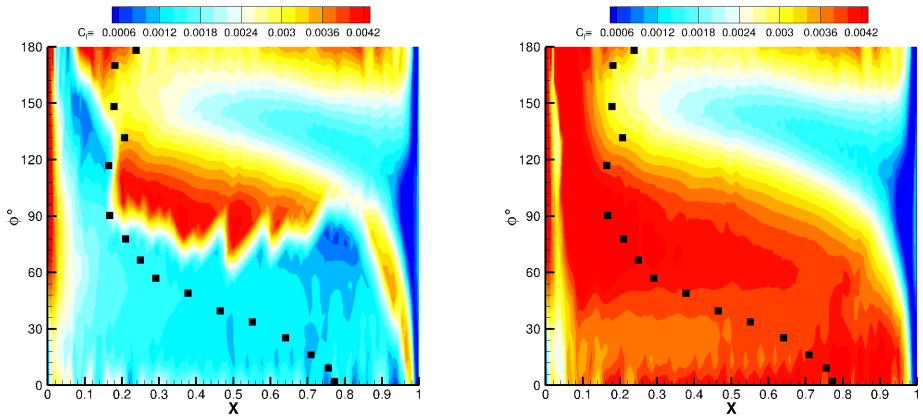

(a) (b)

Fig. 4: Cf distribution in the $x - \phi$ plane for $\frac{\nu_t}{\nu} = 21$ and $Tu = 0.0015$ at the inlet (left) and for $\frac{\nu_t}{\nu} = 250$ and $Tu = 0.005$ at the inlet (right) vs experimental iso$-C_f-$line $C_f = 0.0025$ (black dots).

For what concerns the trigging of crossflow transition, we think that the problem relies on the calculation in Eq.(10) of $\overrightarrow{\phi}$, i.e. the derivative of the vorticity vector, in the first layer of cells next to the wall. An extremely accurate calculation of the second derivative of the velocity is here demanded in order to

activate the criterion and to trigger the crossflow transition.
The second derivative of the velocity is calculated through an Hessian function. Each entrance of the Hessian matrix for a generic quantity Q is built through a least square 2nd order accurate interpolation. Although this Hessian calculation has been demonstrated to be efficient far from the wall, it does not ensure an accurate estimation of the second derivate in the first two layers from the wall where transition is occurring.

4 Conclusion

The presented results made possible to discover some deficiencies of the only Galilean invariant model that is at our disposal in literature, the γ model. All the issues that have been discussed in 2D are mainly related to the implementation of the model. Among all, a not accurate calculation of the velocity derivative normal to the wall can result in an excessive production of turbulence kinetic energy inside the boundary layer. This leads both to an over prediction of the skin friction (flat plate results) and to the not accurate prediction of the transition position isoline, as it is the case for the spheroid on the leeward side. It seems that the choice of the the turbulence model for the coupling (Menter (1994) vs Menter (2003)) does not affect the results, however further investigation should be done for the 3D case. Concerning the crossflow implementation, the main issues are related to the calculation of the second derivative of the velocity in the boundary layer. Extreme accuracy is demanded in the first two layers in order to trigger the transition correlation. Nonetheless, it is necessary to estimate first the physical validity of the included crossflow criterion, then, possibly, to find a new method for the calculation of the second derivatives.
In general, γ-model is extremely sensitive to the inlet parameters. The decay of turbulence kinetic energy ahead of the body strongly affects the numerical results, thus a prior tuning of the input parameters is necessary for a successful computation. Nonetheless, the use of non-physical inlet values, such as enormous values of eddy viscosity ratio to control the turbulence decay, is a topic that is worthwhile to discuss.
In the next future, we are planning to implement the $\gamma - Re_\theta$ model both for Tollmien-Schlichting and crossflow transition.

References

Standard for Verification and Validation in Computational Fluid Dynamics and Heat Transfer. ASME, 2009.

C. Grabe, N. Shengyangand and A. Krumbein (2016) . Transition Transport Modeling for the Prediction of Crossflow transition. 34th AIAA Applied Aerodynamics Conference 2016, Washington D.C., USA.

H.P. Kreplin, H. Vollmers and H.U. Meier (1985). Wall Shear Stress Measurements on an Inclined Prolate Spheroid in the DFVLR 3m x 3m Low Speed Wind Tunnel, Gottingen. DFVLR-AVA, Report Ib 22-84 A 33, 1985.

F.R. Menter, P.E. Smirnov, T. Liu and R. Avancha. A One-Equation Local Correlation-Based Transition Model. *Flow Turbulence Combust*, **95**, 583–619.

`https://www.sharcnet.ca/Software/Ansys/17.0/en-us/help/cfx_thry/i106742654367865.html`